ARTICLE

BIOTECHNOLOGY and BIOENGINEERING

Identification of Highly Selective MMP-14 Inhibitory Fabs by Deep Sequencing

Tyler Lopez, Dong Hyun Nam, Evan Kaihara, Zahid Mustafa, Xin Ge

Department of Chemical and Environmental Engineering, University of California, 900 University Ave, Riverside, California 92521; telephone: 951 827 6229; fax: 951 827 3188; e-mail: xge@engr.ucr.edu

ABSTRACT: Matrix metalloproteinase (MMP)-14 is an important target for cancer treatment due to its critical roles in tumor invasion and metastasis. Previous failures of all compound-based broad-spectrum MMP inhibitors in clinical trials suggest that selectivity is the key for a successful therapy. With inherent high specificity, monoclonal antibodies (mAbs) therefore arise as attractive inhibitors able to target the particular MMP of interest. As a routine screening method, enzyme-linked immunosorbent assays (ELISA) have been applied to panned phage libraries for the isolation of mAbs inhibiting MMP-14. However, because of suboptimal growth conditions and insufficient antibody expression associated with monoclonal ELISA, a considerable number of potentially inhibitory clones might not be identified. Taking advantage of next-generation sequencing (NGS), we monitored enrichment profiles of millions of antibody clones along three rounds of phage panning, and identified 20 Fab inhibitors of MMP-14 with inhibition IC_{50} values of 10–4,000 nM. Among these inhibitory Fabs, 15 were not found by monoclonal phage ELISA. Particularly, Fab R2C7 exhibited an inhibition potency of 100 nM with an excellent selectivity to MMP-14 over MMP-9. Inhibition kinetics and epitope mapping suggested that as a competitive inhibitor, R2C7 directly bound to the vicinity of the MMP-14 catalytic site. This study demonstrates that deep sequencing is a powerful tool to facilitate the systematic discovery of mAbs with protease inhibition functions.

Biotechnol. Bioeng. 2017;114: 1140–1150.

KEYWORDS: matrix metalloproteinase; inhibitory antibody; deep sequencing; synthetic library; bioinformatics

Correspondence to: X. Ge

Contract grant sponsor: National Science Foundation the Faculty Early Career Development (CAREER) Program
Contract grant number: 1453645
Contract grant sponsor: National Institutes of Health
Contract grant number: R01GM115672
Contract grant sponsor: California Breast Cancer Research Program Developmental and Exploratory Award (IDEA)
Contract grant numbers: 21IB-0104; P200A130127
Received 28 September 2016; Revision received 2 January 2017; Accepted 8 January 2017
Accepted manuscript online 16 January 2017;
Article first published online 20 February 2017 in Wiley Online Library (http://onlinelibrary.wiley.com/doi/10.1002/bit.26248/abstract).
DOI 10.1002/bit.26248

Introduction

Matrix metalloproteinases (MMPs) are a class of zinc-dependent endopeptidases responsible for tissue remodeling and extracellular matrix degradation. MMPs play important roles within various aspects of cancer pathology, including tumor growth, metastasis, and angiogenesis (Golubkov et al., 2005; Udi et al., 2015; Zarrabi et al., 2011). In particular, membrane type-1 MMP also known as MMP-14 is a leading factor in cell migration due to its ability to cleave cell surface molecules such as CD44, pro-α_v integrin, and transglutaminase (Baciu et al., 2003; Gingras et al., 2001; Kajita et al., 2001). MMP-14 also processes proMMP-2 into active MMP-2, which promotes the migration of tumor cells (Deryugina et al., 2001; Udi et al., 2015). One of the major challenges with inhibiting MMP-14 as a therapy is the elimination of cross reactivity toward other MMPs. Mounting evidence has suggested that while many facets of MMP proteolytic action are pro-tumorigenic, some MMP family members exhibit tumor-suppressing effects in certain circumstances (Kessenbrock et al., 2010; Overall and Kleifeld, 2006)—for example, MMP-8 favors host defense instead of stimulating tumor proliferation (Decock et al., 2011), and MMP-9 exhibits opposing functions at different microenvironments (Egeblad and Werb, 2002). For these reasons, selectively blocking individual tumorigenesis-promoting MMPs in an appropriate timeframe is highly desired for a successful therapy. However, the catalytic domains of MMP family members share high amino acid similarity and their active sites are extensively conserved. Consequently, development of small molecule inhibitors to distinguish different MMPs is extraordinarily difficult (Zucker and Cao, 2009). Chemical compound inhibitors, for example, hydroxamates, targeting broad-spectrum MMPs all failed in clinical trials due to severe side effects and a lack of efficacy overall (Turk, 2006). The demand for highly selective MMP inhibitors makes monoclonal antibodies (mAbs) an attractive alternative for MMP inhibition (Ager et al., 2015; Bonvin et al., 2015; Devy et al., 2009; Schneider et al., 2012; Sela-Passwell et al., 2011; Smith, 2015).

A panel of inhibitory Fabs targeting MMP-14 with high potency and high selectivity have been isolated from a synthetic human antibody library carrying convex paratopes encoded by long complementarity-determining regions (CDR) H3 regions with 23–27 amino acids, inspired by camelid antibody repertories (Nam et al., 2016). Unlike human or murine antibodies that have

CDR-H3s of 12 and 9 amino acids on average, a large portion of heavy chain antibodies produced by camels or llamas contain long CDR3s that penetrate concave structures of enzyme reaction pockets and inhibit enzymatic functions (De Genst et al., 2006; Desmyter et al., 1996; Forsman, 2008; Lauwereys et al., 1998; Spinelli et al., 1996). Using phage panning and monoclonal ELISA screening, 14 Fabs inhibiting MMP-14 were isolated from the constructed human antibody libraries carrying long CDR-H3 regions. Particularly, Fabs 3A2 and 3D9 exhibited nM potency competitive inhibition toward MMP-14 with no reactivity to MMP-2 or -9 (Nam et al., 2016). However, it has been demonstrated that standard ELISA screenings are incapable of recovering all the antibodies enriched by phage panning or other screening/selection processes (Ravn et al., 2010, 2013), for at least two reasons: (i) slow growth rates of certain enriched clones resulting in low cell density after propagation; (ii) low expression levels of certain antibody proteins resulting in weak ELISA signals.

Next-generation sequencing (NGS) technologies have revolutionized multiple aspects of biological researches (Georgiou et al., 2014; Margulies et al., 2005; Metzker, 2010; Pushkarev et al., 2009), with profound impacts on discovery of specific and functional mAbs (Naqid et al., 2016; Reddy et al., 2010, 2011; Zhu et al., 2013). By high-resolution profiling of an antibody library's diversity, with sequence and frequency information on virtually all clones during screening process, NGS followed by in-depth analysis has been employed to discover many valuable mAbs not found by ELISA screenings (Ravn et al., 2010, 2013; Turner et al., 2016). Encouraged by these studies, we aim to use in-depth analysis to systematically identify and characterize enriched long CDR-H3 clones from our previously panned libraries (Nam et al., 2016). In current study, the DNA samples for Illumina sequencing were prepared without PCR by direct ligation to custom-designed sequencing adapters, which avoid introducing amplification bias. After high-throughput sequencing and bioinformatics analysis, the genes of the 29 most abundant Fab clones in the second and the third rounds of panning (R2 and R3) were rescued. Associated Fabs were then produced and tested for affinity, inhibition, and selectivity (flowchart shown as Fig. 1). Using this technique, we identified 20 inhibitory Fabs, of which 15 were not found by previous ELISA screening. This study demonstrated that, as a supplement to ELISA, deep sequencing is a very powerful tool to facilitate the systematic discovery of antibodies with protease inhibitory functions.

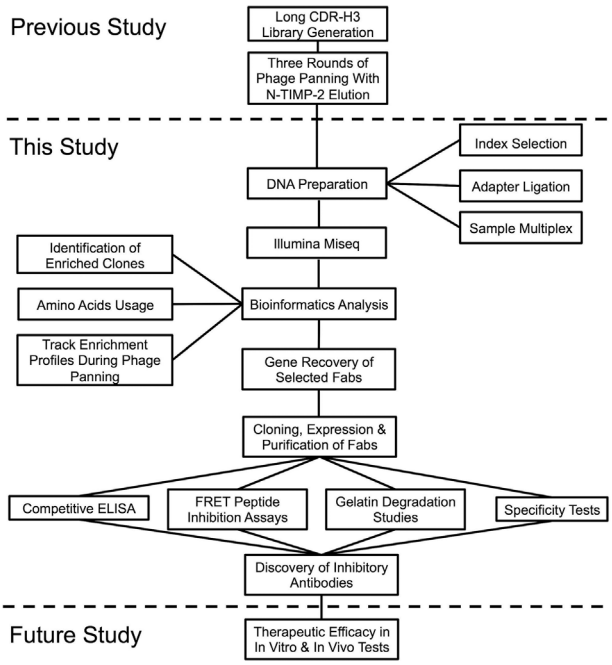

Figure 1. Illumina sequencing and bioinformatics analysis for discovery of inhibitory antibodies. Synthetic antibody libraries carrying long CDR-H3 were constructed and subjected to three rounds of phage panning against cdMMP-14 (previous study, [Nam et al., 2016]). Panned phage libraries were analyzed by deep sequencing to identify Fab clones inhibiting cdMMP-14, and isolated antibodies were characterized biochemically (this study). The therapeutic efficacy of discovered Fabs can be evaluated by vitro and in vivo tests (future study).

Materials and Methods

Preparation of VH Library DNA for Deep Sequencing

Synthetic antibody Fab phage libraries (1.25×10^9 variants) carrying extended CDR-H3 (23–27 amino acids) were constructed and subjected to three rounds of panning (Nam et al., 2016) against the catalytic domain of MMP-14 (cdMMP-14), which was recombinantly expressed (Nam and Ge, 2015), purified, biotinylated, and immobilized on ELISA plates via biotin-BSA and streptavidin. During phage panning, the native competitive inhibitor of MMP-14, TIMP-2 was applied to elute bound phages. For each round of panning (R1, R2, and R3) as well as the original library (Og), *Escherichia coli* cells were infected with the eluted phages and cultured 6 h in 2 × YT supplemented with 100 μg/ml ampicillin. The Fab library plasmids were miniprepped, and double digested with DraIII and BseRI, to isolate the fragments encoding VH FR2-CDR2-FR3-CDR3-FR4 (~280 bp) from gel electrophoresis (Zymo Research, Irvine, CA).

The Illumina sequencing adapters P5 and P7 were customized by introducing a DraIII overhang trinucleotide sequence TGG and a BseRI overhang binucleotide sequence TG at their 5′ and 3′ ends respectively (Fig. S1A). To distinguish DNA samples from various panning rounds, sequencing indexes selected from Illumina's Nextera Kit were used as the barcodes. To maintain an A + C to G + T ratio of 1:1, I5 indexes [N/S/E] 501-504 and I7 indexes N703, N704, N709, and N710 were chosen for library samples Og, R1, R2, and R3, respectively (Fig. S1B). Both strands of modified P5 and P7 adapters containing the selected indexes were synthesized with 5′ phosphorylation (IDT, Coralville, IA), and annealed by gradient cooling from 95°C to 25°C over 45 min in a thermocycler (Bio-Rad, Hercules, CA) to generate double stranded adapters.

Prepared libraries of VH fragments were directly ligated with assembled P5 and P7 adapters via the sticky ends, a non-PCR approach without the introduction of biases caused by amplification. Specifically, 400 ng of DNA at a 10:1 molar ratio of adapters to VH fragments was mixed in a 50 μL reaction containing 1,000 U of T4 DNA ligase (NEB, Ipswich, MA). After incubation at 4°C for 16 h, unreacted adapters were removed from the ligated products (DNA clean up kit, Zymo Research). The purity and concentrations of adapter ligated VH fragments were determined by

spectrophotometry and by RT-qPCR. VH libraries before and after 1–3 rounds of panning were multiplexed based on their concentrations to generate a sequencing mixture with a 10:1:1:1 ratio. After multiplexing the quality of the library was checked using an Agilent 2100 Bioanalyzer.

Bioinformatics Analysis

The multiplexed library was subjected to NGS using a MiSeq sequencer (Illumina, Riverside, CA). Deep sequencing data were analyzed using an automatic bioinformatics pipeline, which combines MATLAB, Perl, Excel, GSplit, and the Windows OS. Large raw FASTQ data files were first split into manageable pieces using GSplit. Each piece was then run through MATLAB to extract the DNA sequences and quality scores. The data were then passed to PERL to isolate high quality sequences containing in-frame CDR-H3 regions. The conserved sequences flanking the CDR-H3 were utilized as the searching motifs for identification of CDR-H3 (Reddy et al., 2010). Each clone was ranked and named according to its library and relative abundancy, for example, clone R2C3 represents the third most abundant clone after two rounds of panning.

Cloning, Expression, and Purification of Fabs

Genes of identified highly abundant Fab clones were PCR amplified from their associated libraries using a universal forward primer recognizing the 5′ of the VL fragment and clone-specific reverse primers matching the unique CDR-H3 sequences. All the primers were designed to have a Tm of 72°C. After initial extraction an extension PCR was performed to amplify and introduce a PpuMI cutting site at the 3′ of the CDR-H3. A Fab phagemid (Farady et al., 2007) was modified to introduce a PpuMI site via a silent mutation immediately downstream of the CDR-H3 region for direct cloning of amplified Fab genes using NsiI/PpuMI restriction sites. Ligated plasmids were cloned into *E. coli* Jude-I [(DH10B) F'::Tn10 (Tet^r)] cells for sequence confirmation, then transformed into BL21 cells for expression.

Fabs containing a 6 × His tag at C-terminal of CH1 were produced by culturing transformed BL21 cells in 2 × YT at 30°C for 15 h. After expression the periplasmic fractions were prepared by osmotic shock with 25% sucrose followed by treatments with lysozyme, EDTA, and $MgCl_2$. Samples were centrifuged at 15,000*g* for 15 min at 4°C to obtain the supernatants containing the Fabs. Periplasmic solutions were then passed through a 0.22 μm filter and purified by using Ni-NTA agarose (Qiagen, Valencia, CA). Purified Fab samples were buffer exchanged into 50 mM HEPES (pH 7.5) by dialysis at 4°C using SnakeSkin tubing (Thermo Scientific, Pittsburgh, PA), and concentrated by using ultrafiltration centrifugation tubes with MWCO of 10 kDa (Amicon, EMD Millipore, Temecula, CA). The purity and concentration of produced Fabs were determined by SDS–PAGE and OD_{280} absorption measurements.

Antibody Characterizations

Dose-Dependent ELISA and Specificity Tests

cdMMP-9, cdMMP-14, and cdMMP-14 mutants were cloned and produced in their active format in periplasmic space of *E. coli* without refolding or activation (Nam and Ge, 2015). After labeling purified cdMMP-14 using EZ-Link Sulfo-NHS-LC biotinylation kit (Thermo Fisher, Lafayette, CO), biotin-cdMMP-14 was incubated in a streptavidin coated ELISA plate (Thermo Scientific) blocked with biotin-BSA. After washing, 50 μL of 2 μM Fabs were then added to the first well and serially diluted to ∼1 nM and incubated for 30 min at 4°C. After washing, the ELISA signals were developed by anti-Fab-HRP (Sigma, St. Louis, MO) and TMB (Thermo Scientific). The color development reaction was stopped by addition of H_2SO_4, and the absorptions at 450 nm were measured. Binding selectivities of Fabs to cdMMP-14 over cdMMP-9 were studied by competitive ELISA. Fabs were incubated with a gradient concentration of cdMMP-9 from 4 μM to 2 nM for 1.5 h at room temperature. After incubation, samples were transferred to an ELISA plate coated with 100 nM cdMMP-14 and processed as described above. Binding kinetics of isolated Fabs were measured by bio-layer interferometry. Using ForteBio BLItz system, biotinylated cdMMP-14 was loaded onto a streptavidin biosensor for 60 s to establish baselines. Fabs were introduced at a variety of concentrations and their association to immobilized cdMMP-14 was monitored for 3 min then allowed to dissociate into 50 mM HEPES (pH 6.8) for 10 min. Determined k_{on} and k_{off} parameters were used to calculate K_D values.

FRET Inhibition Assays

The functionality of purified Fabs to inhibit cdMMP-14 activity was tested by FRET assays. Typically, 1 μM of purified Fab was serially twofold diluted into assay buffer (50 mM Tris-HCl pH 7.5, 150 mM NaCl, 5 mM $CaCl_2$, 0.5 mM $ZnCl_2$), and incubated with 10 nM cdMMP-14 for 30 min at 4°C. The kinetic measurements were started with the addition of 1 μM M2350 peptide substrate (Bachem, Torrance, CA) and the fluorescence was monitored with excitation and emission wavelengths at 325 and 392 nm. To determine the type of inhibition Fabs were diluted to concentrations generating 70%, 50%, and 30% inhibition in HEPES assay buffer (50 mM HEPES pH 6.8, 150 mM NaCl, 5 mM $CaCl_2$, 0.5 mM $ZnCl_2$), and incubated with 10 nM cdMMP-14 at 4°C for 30 min. For each Fab concentration, 50 μM to 2 mM FRET peptide substrates were added for kinetics measurements.

Table I. Statistics of deep sequencing results.

	Raw data	In-frame full-length CDR-H3s	In-frame full-length/raw data (%)	Unique CDR-H3s	Unique/in-frame full-length (%)	Frequency (copy numbers) of the most abundant clone
Og	2,039,671	1,834,712	89.95	1,834,576	99.99	0.000% (2)
R1	19,488,812	10,941,297	56.14	10,791,087	98.63	0.009% (981)
R2	11,761,506	6,665,700	56.67	6,229,221	93.45	0.129% (8600)
R3	50,457	28,127	55.74	19,906	70.77	1.888% (531)

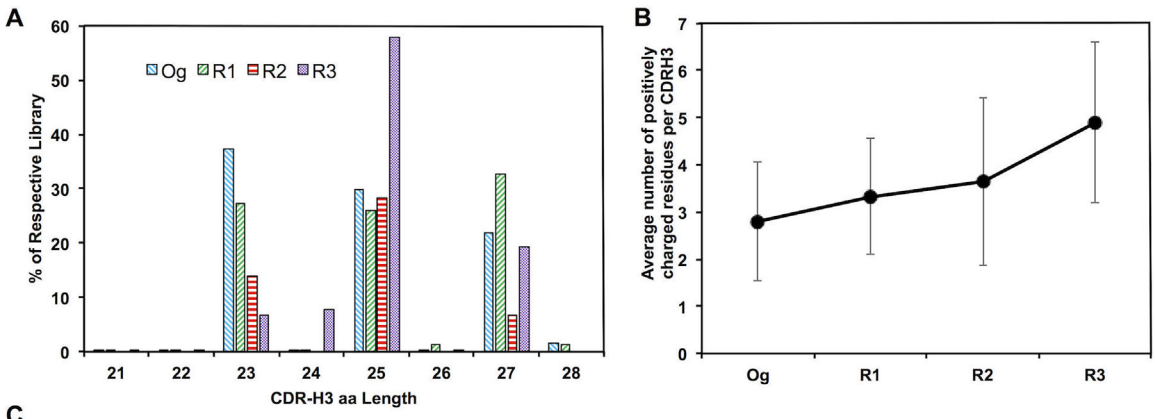

C

	92	93	94	95	96	97	98	99	100	100A	100B	100C	100D	100E	100F	100G	100H	100I	100J	100K	100L	100M
Positively Charged	-11	-14	28	-3	6	15	-7	28	25	-5	-7	29	17	-2	-2	1	2	-4	0	15	2	0
Negatively Charged	-11	2	-5	-4	4	0	-6	-6	-4	-6	-5	-5	-6	-4	-4	-2	-4	22	-5	-2	8	1
Polar	24	13	-4	-8	30	22	0	11	-12	-6	33	11	15	18	-10	5	-5	12	10	-5	6	0
Hydrophobic	-19	8	-5	2	-31	-25	23	-27	2	19	-18	-26	-20	-2	0	5	20	-27	-6	-22	-19	-12

Figure 2. Antibody repertoire analysis of phage panned long CDR-H3 libraries. (**A**) CDR-H3 length distribution. (**B**) Enrichment of positively charged residues (R, H, K) at CDR-H3. (**C**) Amino acid composition changes at each position (92–100 M) of CDR-H3 with 25 aa. Residues were grouped according to biochemical properties: positively charged (R, H, K), negatively charged (D, E), polar (S, T, N, Q), and hydrophobic (A, I, L, M, F, W, Y, V). The percentage changes from the library Og to R3 are listed, positions with >20% change were highlighted in bold boxes.

Gelatin Degradation Studies

A total of 10 nM cdMMP-14 was incubated with 1 mg/mL gelatin (porcine skin, Sigma) in the absence or presence of 1 μM Fabs for 24 h at room temperature, then samples were analyzed by 12% SDS–PAGE. A synthetic inhibitor GM6001 and a non-inhibitory Fab R2C17 were used as the positive and negative controls.

Results

Illumina Deep Sequencing of Long CDR-H3 Fab Libraries

Human Fab phage display libraries carrying CDR-H3 regions with 23, 25, and 27 aa in length were synthesized and subjected to three rounds of panning (R1, R2, and R3) against catalytic domain of MMP-14 (cdMMP-14) (Nam et al., 2016). For each round, the bound phages were eluted by incubation with n-terminal domain of tissue inhibitors of metalloproteinases (n-TIMP-2), which is a native inhibitor of MMP-14 behaving in a competitive mode (Brew et al., 2000). In principle, only the Fab phages directly interacting with the catalytic portion of MMP-14 or allosterically interfering n-TIMP-2 binding can be eluted off. Therefore, the combination of convex paratope library design with epitope-specific elution presumably results in enrichment of specific inhibitory antibodies. This hypothesis was partially confirmed by the panel of inhibitory Fabs isolated by ELISA screening in our previous study (Nam et al., 2016). Aiming to fully understand the sequence landscape changes during the panning process and to systematically identify and characterize a large number of the most enriched antibody clones, libraries R1, R2, R3, and the original library before panning (Og) were subjected to Illumina NGS (Fig. 1). Briefly, Og, R1, R2, and R3 phagemids were purified, and their fragments encoding CDR-H3s with partial FR3 and FR4 regions were prepared by restriction digestion and direct ligation with custom-designed adapters for Illumina sequencing (Fig. S1). This PCR free procedure should minimize the introduction of amplification bias, which is critical for frequency based antibody discovery (Ravn et al., 2010, 2013; Reddy et al., 2010, 2011; Zhu et al., 2013). RT-qPCR analysis showed that the assembled DNA samples had uniform melting temperatures, suggesting high quality and purity. The library DNA concentrations were quantified and the samples were multiplexed at a ratio of 10:1:1:1 (Og:R1:R2:R3) for sequencing. Analysis on an Agilent 2100 bioanalyzer further confirmed that the multiplexed DNA sample displayed sharp peaks associated with designed lengths, indicating successful ligations with the flow cell adapters at both ends.

Sequencing raw data was de-multiplexed using unique indexes and processed in house to remove truncated and out of frame reads. Sequences either containing reading frame shifts due to sequencing errors or with low quality (quality scores less than 30) were excluded from further analysis. A total of 1.83×10^6, 1.09×10^7, 6.67×10^6, and 2.81×10^5 functional sequences were obtained for libraries Og, R1, R2, and R3 respectively, which accounted for 56–90% of the raw data (Table I). Given that the library diversity usually decreased to $<10^5$ after the first round of biopanning, the Illumina results provided a considerable coverage and well represented the majority of R1, R2, and R3 library clones. The large diversity of Og (1.25×10^9) was not covered by NGS, nevertheless $>10^6$ reads are adequate to probe the quality of constructed library.

Long CDR-H3s Enriched With Hydrophilic and Positively Charged Residues After Panning on cdMMP-14

As the most important region of antigen binding, CDR-H3s were focused for bioinformatics analysis (Fig. 1). Their sequences were recognized by using the signature motifs flanking N- and C-termini

Table II. In depth analysis of highly enriched clones from R2 and R3.

ID by NGS[a]	Sequence (CDR-H3 length)	% of R2	% of R3	Rank in R3	Binding affinity[b]	Inhibition potency	Yield (mg/L)
R2C1*	STAATTLSRMSRSYWTIQLPYGMDY (25)	**0.13**	1.89	1	590 nM	Non-inhibitory	1
R2C2*	GVRGNKLRLLSSRSGLMESHYVMDY (25)	**0.12**	1.66	2	1.0 μM	2.3 μM	2
R2C3*	PTTSRVNKKLFRVSVLHPGSYGMDY (25)	**0.11**	0.61	4	220 nM	4.6 μM	1
R2C4	GWRVYADRGHVRGYFRVWYGMDY (23)	**0.10**	0.53	3	10 μM**	1.5 μM	2
R2C5	IMKIKRNSLKFRGFVPLQMQYVMDY (25)	**0.09**	0.14	14	375 nM**	50 nM	3.5
R2C6	KDLLKTNRLTTRYKKSVSVGYGMDY (25)	**0.07**	0.53	5	2.4 μM	2.4 μM	1
R2C7	SCVWACCACRYWSGSDSHYAMDY (23)	**0.06**	0.01	~12,500	153 nM	100 nM	1
R2C8	PGRHLQTTFKGYQFKYSRYIYAMDY (25)	**0.05**	0.16	12	1.2 μM	1.2 μM	3.5
R2C9	VLNIFMDVGAARFPGLVRYGMDY (23)	**0.04**	0.05	~4,200	657 nM**	80 nM	0.75
R2C10	MAKDFRILASVRMWVLASRLYVMDY (25)	**0.04**	0.03	~8,400	360 nM	Non-inhibitory	0.5
R2C11	RYGSDVFCVGCFFGVRLSYVMDY (23)	**0.03**	0.03	~9,100	750 nM	600 nM	0.75
R2C12	SDSWVQGRDFCYYSAWVGYGMDY (23)	**0.03**	0.05	~2,600	150 nM	150 nM	0.5
R2C13*	LYNGWLMVEGIGSAREGPTWYAMDY (25)	**0.03**	0.09	21	34 nM	970 nM	< 0.01
R2C14	VSNRYNRSSASIAGLQLFRPYGMDY (25)	**0.03**	0.05	~2,600	1.2 μM**	10 nM	0.5
R2C15*	SVHMKLSNKILSGWSWNNSFYAMDY (25)	**0.03**	0.07	28	460 nM	3.9 μM	2
R2C16	FKNADFAAGGQWSKMLIARMYAMDY (25)	**0.03**	0.10	17	1.8 μM	5.5 μM	2.4
R2C17	VGAWRVPSERMFTYPSARTRYAMDY (25)	**0.03**	0.02	~11,000	2.1 μM	Non-inhibitory	0.4
R2C18	RDFGGFAGCLDGYVHVCWYAMDY (23)	**0.02**	<0.01	~13,000	430 nM	Non-inhibitory	0.5
R2C19*	LDRDRYIHVGRAGNTYSNYYYVMDY (25)	**0.03**	0.17	11	9.7 nM	Non-inhibitory	0.5
R2C20*	NFRVESAGRPGKTVLRKDGKYAMDY (25)	**0.03**	0.47	6	1.6 μM	Non-inhibitory	0.5
R2C21	LAWKSDNRGSFAKLQFTLKMYGMDY (25)	**0.02**	0.08	25	Non-binding**	50 nM	0.25
R2C22	HSRDGWQHWFGNWAGLHSYGMDY (23)	**0.02**	<0.01	~13,000	540 nM**	75 nM	0.15
R3C7*	EIHMLSRQARYLRDGRRPRGSMYVMDY (27)	0.01	**0.33**	7	29 nM	Non-inhibitory	2
R3C8	HCLLRSRRCEMSTKTRELNVYRYAMDY (27)	0.01	**0.30**	8	1.3 μM	5.4 μM	1
R3C9*	VKLQKDKSHQWIRNLVATPYGRYVMDY (27)	0.01	**0.29**	9	3.8 nM	9.7 nM	1
R3C10	GSLRRDFNLVVRSSWDIRSNYVMDY (25)	<0.01	**0.20**	10	970 nM	1.0 μM	2
R3C13	WLRVSLKSGVYKVLARAVELDEYVMDY (27)	0.01	**0.14**	13	2.0 μM	2.0 μM	3
R3C15	GVRGNKLRLLSSRSGRMESHYVMDY (25)	<0.01	**0.14**	15	57.5 nM	170 nM	4
R3C16	MASIDLRMLSRMLAGPQFKVYGMDY (25)	0.01	**0.11**	16	Non-binding**	1.0 μM	1

[a]Clones were identified and ranked by their abundancies in their respective libraries (bold numbers). Previously discovered Fabs by monoclonal phage ELISA are labeled as *.

[b]Fab genes were rescued by PCR and sub-cloned for expression. Purified Fabs were tested for binding affinity (by ELISA EC_{50}) and inhibition potency (by FRET IC_{50}). Fabs with $EC_{50} > 2 \times IC_{50}$ are labeled as **.

of CDR-H3s (Ravn et al., 2010; Reddy et al., 2010). Analysis results indicated that the original library as expected, contained an even distribution of CDR-H3s with 23, 25, or 27 aa (30–37% each). Interestingly, after phage panning more than half of Fabs (58%) had 25 aa in their CDR-H3s, and the proportions of CDR-H3s with 23 or 27 aa decreased to 7% and 19% (Fig. 2A). Taking 25 aa CDR-H3s as an example, at each position of 92–100 K, the Og library showed uniform usage of 20 amino acids (Fig. S2), indicating constructed synthetic antibody libraries had high quality and well represented the diversity designs. During the panning process, CDR-H3 amino acid usage distributions altered dramatically (Fig. S2). Particularly, the average number of positively charged residues (Arg/His/Lys) steadily increased from 2.8 aa per CDR-H3 in Og to 3.3 in R1, 3.6 in R2, and finally 4.9 in R3 (Fig. 2B). This suggests the panning process enriched positively charged paratopes, which probably enhances interactions with the negatively charged MMP-14 catalytic cleft vicinity (Fernandez-Catalan et al., 1998). The usages of amino acids grouped according to physicochemical properties were further analyzed at individual residue positions of CDR-H3s. Results for CDR-H3s with 25 aa are shown in Figure 2C, in which changes of 20% and more from Og to R3 are highlighted. Positively charged residues were enriched at positions 94, 99, 100, and 100 C; proportions of negatively charged residues (Asp/Glu) increased at position 100I; polar residues (Ser/Thr/Asn/Gln) presented more at positions 92, 96, 97 and 100B; and hydrophobic residues (Ala/Ile/Leu/Met/Phe/Trp/Tyr/Val) presented less at position 96, 97, 99, 100C, 100D, 100I, and 100 K. Overall, the increase of charged and hydrophilic residues with decrease of hydrophobic residues presumably improves Fab solubility, a phenomenon well documented in literature (Chiti et al., 2003; Lawrence et al., 2007; Nieba et al., 1997).

Identification of Highly Abundant Fab Clones and Tracking Their Enrichment Profiles

After bioinformatics analysis of the entire libraries in general, individual Fab clones with the highest abundancies were identified for further studies. Limited by Illumina reading length capacity, the most diverse regions, CDR-H3s were chosen as the signature sequences to represent the associated Fabs in analysis, and the full VH and VL sequences of particular clones of interest were later recovered by PCR using specific primers. For libraries Og, R1, R2, and R3, a total of 1.83×10^6, 1.08×10^7, 6.23×10^6, 1.99×10^4 different CDR-H3s were found (unique CDR-H3s, Table I). The ratios between numbers of unique CDR-H3s over numbers of all in-frame full-length CDR-H3s in the associated library are 99.99% for Og, 96.63% for R1, 93.45% for R2, and 70.77% for R3. The copy numbers of each unique CDR-H3 sequences within R1, R2, and R3 were then counted, and their abundancies were calculated by dividing their copy numbers with the total number of functional CDR-H3s in that library (Table I). Results demonstrated that the most abundant clones in R1, R2, and

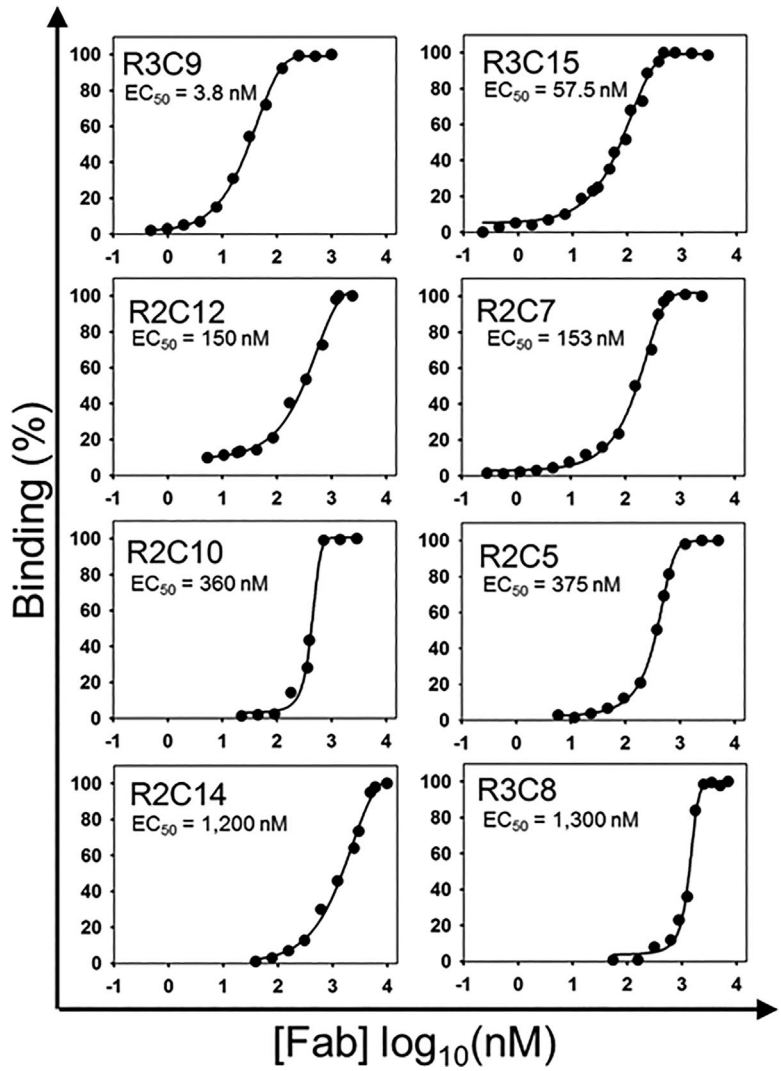

Figure 3. Fab binding affinities measured by ELISA. ELISA studies were performed by reacting purified Fabs with immobilized cdMMP-14 followed by tagging with anti-Fab-HRP. Color was then developed by the addition of TMB and read on a spectrophotometer. A range of binding strengths from 4 nM to 10 μM was found, which is expected from a synthetic antibody library.

R3 had frequencies of 0.009%, 0.129%, and 1.889%, respectively, reflecting the quick enrichment progress during panning as expected. Because R1 enrichment was pre-mature, only R2 and R3 were used for Fab identification in the following analysis.

Due to the synthetic nature and relatively small dataset (1.83×10^6) of Og library compared to constructed diversity (1.25×10^9), majority of clones in Og presumably should have a single copy number. Our results indeed indicated that 99.99% of Og CDR-H3s had a single copy, <0.01% CDR-H3s have two copies and there are no clones with more than two copies (Table I), suggesting each clone in Og has a low and even frequency. Consequently, the enrichment of a given clone in R1, R2, or R3 over Og can be directly reflected by their frequencies in the associated library, therefore, the clones with the highest abundancies are the most enriched clones. The 22 most abundant clones in R2 were identified with frequencies ranging from 0.13% to 0.02% (named as R2C1-R2C22 with their CDR-H3 sequences shown in Table II). None of these 22 clones were detected in Og (zero copies). In R1, the majority of these 22 clones had zero copies and only R2C3 and R2C19 had one copy.

Notably, the ranks and abundancies of these 22 clones in R2 were not always correlated with these in R3. More specifically, 15 clones such as R2C3, R2C4, and R2C6 exhibited further enrichments, that is, a higher abundancy in R3 than R2. Because of this enrichment pattern, 7 of the 22 most abundant clones were discovered using traditional ELISA screening (Table II, Table S1) (Nam et al., 2016). Clones R2C9, R2C10, and R2C17 displayed increased frequencies from Og to R1 and to R2, however, their frequencies in R3 were similar to R2. These plateaus can be attributed to the balance between enrichment driven by panning and the depletion caused by slow cell growth. Interestingly, several top ranked clones in R2 such as R2C7, R2C18, and R2C22

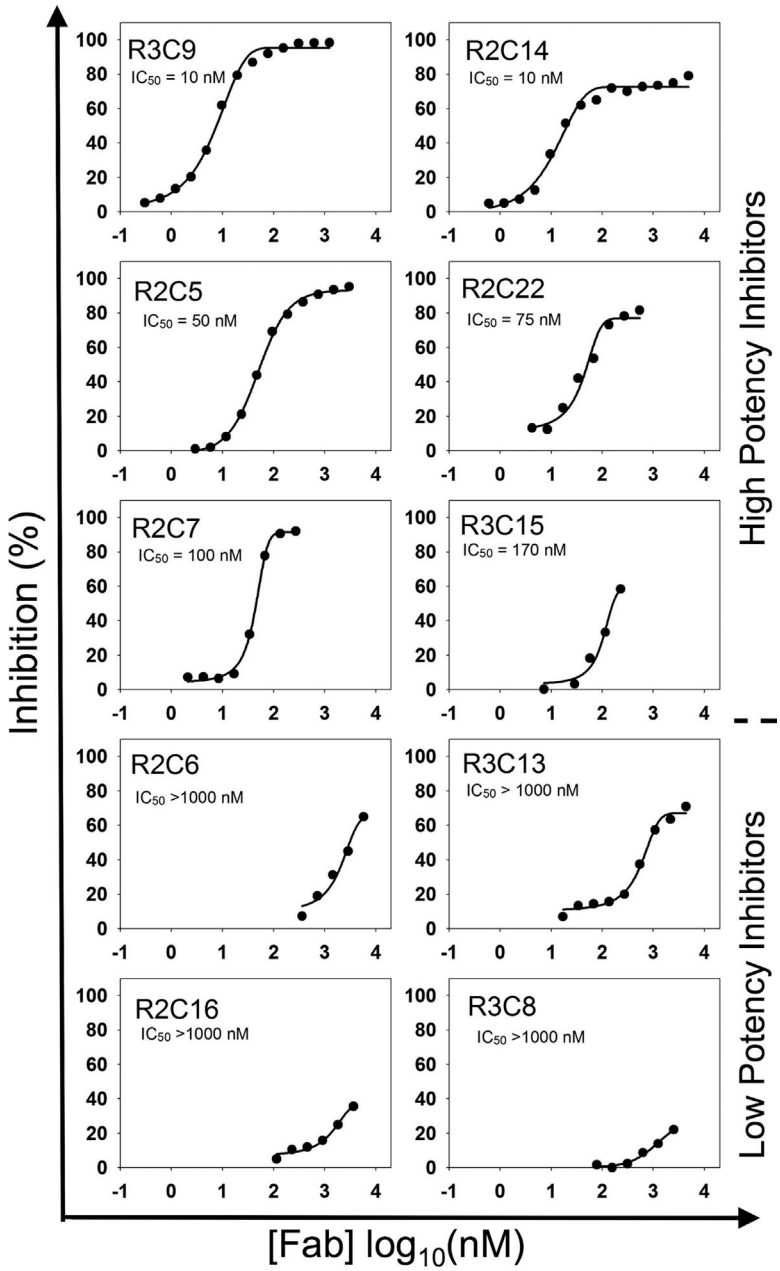

Figure 4. Potencies of inhibitory Fabs by FRET assays. FRET assays were performed by reacting the purified Fabs with cdMMP-14 for 30 min then adding FRET peptide substrate. The increase in fluorescence was monitored for 1 h to determine inhibitory function. A variety of inhibitory clones with potencies ranging from 10 nM to 8.0 μM was found.

showed declined frequencies in R3. As a consequence, these particular clones were not identified in ELISA screenings of R3 library, because of their low frequencies in R3 (<0.01% with rankings >10,000, Table II).

Applying similar analysis, the 17 most abundant clones from R3 were also identified with frequencies ranging from 1.89% to 0.11%. For these 17 clones, seven were not among the top 22 clones of R2. These seven clones were named as R3Cx, in which x is the rank of that clone in R3. All R3Cx clones were undetected in Og or R1, had relatively low frequencies in R2 (<0.01%), and quickly enriched in R3 (0.33–0.11%).

Gene Rescue and Protein Production for Abundant Fabs

Fab genes of these 29 top ranked clones (22 from R2 and 7 from R3) were specifically amplified from their respective libraries by PCR using a universal forward primer recognizing N-terminal of the VL and a clone specific reverse primer recognizing unique CDR-H3s. After secondary extension PCR to introduce a restriction site at the C-terminal of VH, the VL-CL-VH fragments were sub-cloned into a Fab expression plasmid. Successful gene extraction and cloning were confirmed by Sanger sequencing. The Fabs were produced in the periplasmic space of *E. coli* with typical 0.5–2.0 mg purified proteins

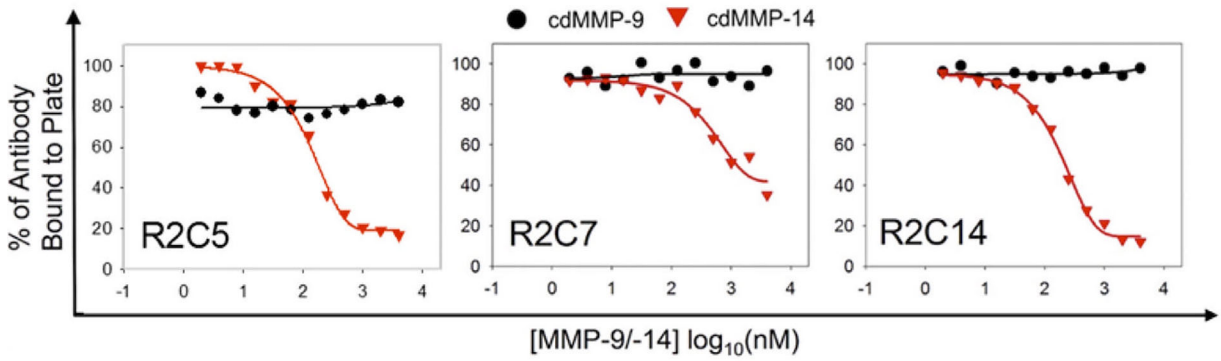

Figure 5. Specificity tests by competitive ELISA. Fabs at their respective IC_{50} concentrations were incubated with varying concentrations of cdMMP-9 or cdMMP-14 then added to ELISA plates coated with 100 nM cdMMP-14. Fabs bound to the cdMMP-14 on plates, even at high concentrations of cdMMP-9, indicating there are no interactions between Fabs and cdMMP-9. As the control experiments, when incubating with cdMMP-14 in solution, Fabs transferred from the plate to the solution as the concentration of cdMMP-14 in solution increased.

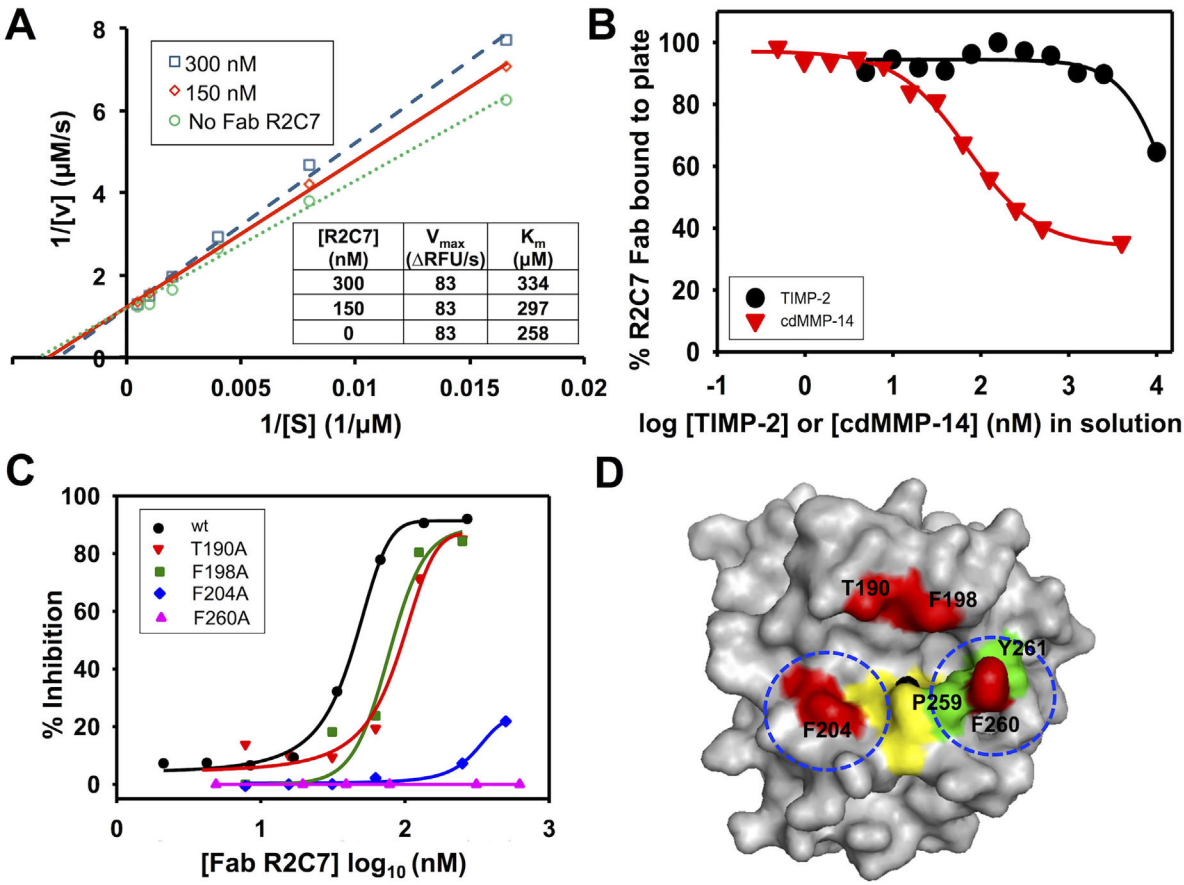

Figure 6. Inhibition mechanism of R2C7. (**A**) Lineweaver–Burke plots of cdMMP-14 at the presence of 0, 150, 300 nM Fab R2C7. Unaltered V_{max} and increased K_m with increasing Fab concentrations indicate a competitive inhibition mode. (**B**) Competitive ELISA with TIMP-2. Fab R2C7 was mixed with varying concentrations of TIMP-2 in solution before addition to an ELISA plate coated with 100 nM cdMMP-14, and the signals were developed by using anti-Fab-HRP and the associated substrate. (**C**) R2C7 epitope mapping by inhibition assays. Four positions T190, F198, F204, and F260 surrounding the catalytic cleft of cdMMP-14 were chosen for alanine mutagenesis. Compared to wt cdMMP-14, F260A, and F204A cannot be inhibited by Fab R2C7. (**D**) R2C7 epitope image generated using PyMOL based on MMP-14 crystal structure (PDB 1bqq), showing the catalytic zinc (solid black), site-directed mutagenesis positions (red), the three histidine residues of the catalytic motif HEXXHXXGXXH (yellow), and the residues forming the wall of S1′ cleft (green, except F260 which is also a mutation site thus in red). Determined locations of R2C7 binding are circled.

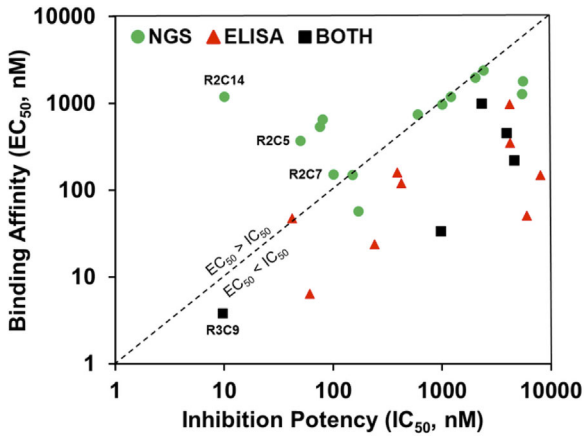

Figure 7. Relationship between binding affinity and inhibition potency. The clones found by NGS (green circles), phage ELISA (red triangles), or both methods (black squares) are compared. The diagonal dashed line represents equal EC_{50} and IC_{50} values.

per liter of culture medium (Table II), yields sufficient for initial biochemistry characterizations. Most top ranked clones exhibited relatively high expression levels compared to the lower ranked clones, suggesting expression level is an important factor affecting enrichment progress during phage panning. Purified Fabs remained stable and functional at room temperature for at least 24 h.

Discovery of a Panel of Inhibitory Fabs With High Selectivity

The binding affinities of purified Fabs were measured by ELISA and results indicated that majority of highly abundant clones (27/29) exhibited binding specificity to cdMMP-14 with EC_{50} values ranging from 4 nM to 3 μM (Table II, Fig. 3). Among them, eight Fabs R2C1, R2C3, R2C12, R2C13, R2C19, R3C7, R3C9, R3C15 had relatively high affinities at 4–150 nM; five Fabs R2C5, R2C7, R2C10, R2C15, and R2C18 exhibited moderate affinities at 150–500 nM; and 14 other Fabs showed weak binding with EC_{50} values at 0.5–3 μM. Given these Fabs were isolated from synthetic phage libraries, a broad range of affinities was expected.

More importantly, inhibition functions of the purified Fabs on cdMMP-14 were examined using a FRET peptide substrate to derive IC_{50} curves (Fig. 4). Of the 29 highly abundant Fab clones identified from R2 and R3, 20 exhibited inhibition with IC_{50} values ranging from 10 nM to 4 μM (Table II). Particularly, R2C14 and R3C9 had an inhibition potency of 10 nM; eight Fabs R2C5, R2C7, R2C9, R2C12, R2C13, R2C21, R2C22, and R3C15 exhibited inhibition potencies at 50–200 nM; and 10 other Fabs had weak inhibition with IC_{50} 600 nM–4 μM.

Three Fabs R2C5, R2C7, and R2C14 of high and moderate inhibition potencies (10–100 nM) but not found by ELISA screening in previous study were further characterized for their binding selectivity to cdMMP-14 over highly homologous cdMMP-9. Tests were performed by incubating Fabs at their IC_{50} concentrations with varying concentrations of cdMMP-9 or cdMMP-14 then adding to an ELISA plate coated with streptavidin and biotinylated cdMMP-14. Fabs R2C5, R2C7, and R2C14 bound to cdMMP-14 on the plate even with high concentrations of cdMMP-9 in solution, indicating no interactions with cdMMP-9 (Fig. 5). While in control experiments, the amounts of Fabs binding to immobolized cdMMP-14 responded to concentrations of cdMMP-14 in solution as expected. Therefore, Fabs R2C5, R2C7, and R2C14 exhibited high selectivity to cdMMP-14. A further zymography test of Fab R2C7 also demonstrated that it inhibited cdMMP-14 from degrading gelatin (Fig. S3).

Inhibition Mechanism of R2C7

To determine the type of inhibition, a series of enzymatic activity assays in the presence of 0, 150, and 300 nM Fab R2C7 were performed. The obtained Lineweaver-Burk plots demonstrate an unchanged turnover rate (V_{max}) and an increased Michaelis constant (K_m) when Fab concentration was raised, indicating a competitive inhibition mode (Fig. 6A). Competitive ELISA with increased concentrations of n-TIMP-2 resulted in decreased amounts of Fab R2C7 bound to immobilized cdMMP-14 (Fig. 6B), suggesting that R2C7 and n-TIMP-2 directly competed on binding to cdMMP-14, and presumably their epitopes were at least partially overlapping. As the control experiments, when incubating with cdMMP-14 in solution, Fabs transferred from the solution to the plate as the concentration of cdMMP-14 in solution decreased to ~10 nM.

To further determine whether R2C7 is a direct or allosteric competitive inhibitor, binding site of Fab R2C7 was studied by alanine scanning mutagenesis of MMP-14. Four residue positions around reaction pocket of cdMMP-14 (T190A, F198A, F204A, and F260A) were selected for Ala substitution, and these cdMMP-14 mutants were prepared by periplasmic expression without refolding (Nam and Ge, 2015). Inhibition assays with FRET peptide substrate indicated that R2C7 lost its inhibition ability toward cdMMP-14 mutants F204A and F260A, while keeping the same level of inhibition potency toward T190A and F198A as wild-type cdMMP-14 (Fig. 6C). Notably, F204 and F260 are responsible for the formation of a relatively deep S1′ site of MMP-14 among MMP family (Chiti et al., 2003, Nagase, 2001), suggesting R2C7 binds to the reaction pocket vicinity of cdMMP-14 directly (Fig. 6D).

Discussion

Next generation high-throughput sequencing is a powerful tool for analyzing rounds of selected libraries, which led to the identification of unique inhibitory antibodies in current study. In conjugation with convex paratope antibody library design, an n-TIMP-2 elution method was used during the phage panning process to enrich the libraries in competitive inhibitory clones. Traditional ELISA screenings were performed on the third round panned library by randomly picking individual colonies. This method resulted in the discovery of some of the most abundant clones in R3, as well as a few random clones that were not necessarily abundant but nonetheless picked (Table S1). However, some clones enriched in R2 but declined in R3 will likely be missed in ELISA screening. For example, the seventh most abundant clone in R2, R2C7 is ranked ~12,500 in R3 with a frequency of 0.01%. Clones such as R2C7 (with an inhibition potency of 100 nM), are

valuable candidates for further development but are depleted in continual rounds of panning. Applying ELISA on R2 is not realistic either, because even the most enriched clones in R2 had a frequency of ~1/1,000. By NGS, laborious ELISA screenings is avoided and all enriched clones with their abundancies above the background can be identified and tracked along rounds of the panning process. Using this approach, many valuable clones with high inhibition potencies, such as R2C7, R2C9, R2C12, and R2C22, were newly discovered. In fact, 15 of 20 identified inhibitory Fabs were not found by ELISA, demonstrating the power of NGS.

Because only a trace fraction of Og was sequenced, all of the 29 highly abundant clones identified from R2 and R3 have zero copies in Og. Therefore their frequencies in R2 and R3 can be directly used to reflect their enrichment over Og. By tracking their frequencies during phage panning process, we found three patterns—rise, plateau, and decline (TOC). The observed different enrichment and depletion patterns occur because phage panning is a multi-step process involving cell growth, Fab expression and display, and competitive binding. Suboptimal conditions at any of these steps can result in a decrease of abundancy. For example, an individual clone that grows slowly will be overtaken and gradually phased out by its faster growing competitors. This effect has nothing to do with the strength of the antibody, however, it will still result in the stagnation or depletion of the clone relative to the total library in subsequent rounds of panning. Another major concern during the phage ELISA selection process is low expression levels of antibody molecules. A clone that binds strongly, but does not express well may not have a high enough signal to be selected; this results in the loss of the clone. Finally, individual clones will compete for binding sites on the bound MMP-14. This results in the loss of weaker binding yet potentially inhibitory clones.

The 20 MMP-14 binding Fabs identified by ELISA in previous study were also tracked to monitor their enrichment profiles. As results shown in Table S1, 9 of the 20 clones were among the most abundant 29 clones identified by NGS. The remaining 11 clones have frequencies less than 0.01% in R2 and less than 0.05% in R3, thus were not discovered by frequency-based NGS and bioinformatics, but randomly picked by monoclonal ELISA. To better understand the Fab populations isolated by ELISA, or NGS, or both methods, the correlations between binding affinity (ELISA EC_{50}) and inhibition potency (FRET assay IC_{50}) of each Fabs were plotted. As shown in Figure 7, most of the Fabs generated by ELISA screening have their EC_{50}s less than their IC_{50}s, whereas a few inhibitory Fabs identified by NGS, for example, R2C5 and R2C14, exhibited higher affinity EC_{50} values than inhibition IC_{50} values. A likely explanation of this phenomenon is that these Fabs are suicide inhibitors (Farady et al., 2007), which are slowly cleaved by high concentrations of cdMMP-14 after incubation for hours (SDS–PAGE results shown in Fig. S4). To further characterize these selected Fabs, their binding kinetics k_{on} and k_{off} parameters were measured by bio-layer interferometry. Data indicated that Fabs R2C5, R2C7, and R2C14 had calculated K_D values of 15.3, 27.0, and 6.1 nM (Fig. S5), which were less than their inhibition IC_{50}s (50, 100, and 10 nM, respectively). Collectively these results suggest that the low apparent binding affinities measured by ELISA were attributed to slow cleavage of Fabs by immobilized cdMMP-14 on ELISA plates, while the quick and real-time analysis by bio-layer interferometry can measure the binding kinetics before significant cleavage takes place. Guided by the knowledge of theoretical cut sites of MMP-14, for example, usually containing a positively charged residue at the P4 position and a hydrophobic residue at the P1′ position (Kridel et al., 2002), studies on site-specific mutagenesis are currently undertaken to engineer cleavage resistant Fabs.

Avoiding sequencing artifacts is critical for the success of frequency-based antibody discovery. PCR often introduces bias due to the differential amplification of some DNA templates over others. In this study, sequencing adapters were custom-designed for direct ligation with antibody CDR-H3 fragments prepared by phagemid extraction and restriction digestion. This procedure without amplification presumably minimized quantification biases caused by PCR.

In conclusion, combination of the convex paratope antibody library design with next-generation deep sequencing of panned libraries allowed us to identify a panel of highly potent and highly selective Fabs inhibiting cdMMP-14 not found by ELISA. Particularly, Fab R2C7 exhibited 100 nM inhibition potency by binding to the catalytic cleft vicinity of cdMMP-14. In addition to R2C7, several potent inhibitory Fabs for example, R2C5 and R2C14, with IC_{50} values at 10–50 nM with excellent selectivity were also isolated. And Fabs R2C5, R2C9, R2C12, R3C15 were found to be competitive inhibitors as well. This panel of inhibitory Fabs provides us a rich pool of lead candidates for further selection of suitable epitopes for therapeutics and optimization of pharmacological properties through affinity maturation and solubility/stability improvement. Besides MMP-14, several other MMP family members have been recognized playing important roles in variety of indications, therefore the methodology demonstrated in the current study can be readily applied for the generation of highly potent inhibitory mAbs targeting other MMPs or serine proteases (Farady et al., 2007; Schneider et al., 2012) of physiological significance. These highly selective inhibitors can also been used as research tools for better understanding of the not well-defined network of MMPs with their substrates.

This work was supported by National Science Foundation the Faculty Early Career Development (CAREER) Program 1453645, National Institutes of Health Grant R01GM115672, and California Breast Cancer Research Program Developmental and Exploratory Award (IDEA) 21IB-0104. T.L. is partially supported by Department of Education Graduate Assistance in Areas of National Need (GAANN) program. We would like to thank Dr. John Weger at UCR Genomics Center for help with Illumina sequencing adapter designs. We would also like to acknowledge the contributions of undergraduate researchers Chris Benitez, Henry Pham, Aaron Ramirez, and Ramon Sanchez.

References

Ager EI, Kozin SV, Kirkpatrick ND, Seano G, Kodack DP, Askoxylakis V, Huang Y, Goel S, Snuderl M, Muzikansky A, Finkelstein DM, Dransfield DT, Devy L, Boucher Y, Fukumura D, Jain RK. 2015. Blockade of MMP14 activity in murine breast carcinomas: Implications for macrophages, vessels, and radiotherapy. J Natl Cancer Inst 107(4):djv017.

Baciu PC, Suleiman EA, Deryugina EI, Strongin AY. 2003. Membrane type-1 matrix metalloproteinase (MT1-MMP) processing of pro-αv integrin regulates cross-talk between αvβ3 and α2β1 integrins in breast carcinoma cells. Exp Cell Res 291:167–175.

Bonvin P, Venet S, Kosco-Vilbois M, Fischer N. 2015. Purpose-oriented antibody libraries incorporating tailored CDR3 sequences. Antibodies 4:103–122.

Brew K, Dinakarpandian D, Nagase H. 2000. Tissue inhibitors of metalloproteinases: Evolution, structure and function. Biochim Biophys Acta 1477(1-2):267–283.

Chiti F, Stefani M, Taddei N, Ramponi G, Dobson CM. 2003. Rationalization of the effects of mutations on peptide and protein aggregation rates. Nature 424:805–808.

De Genst E, Silence K, Decanniere K, Conrath K, Loris R, Kinne J, Muyldermans S, Wyns L. 2006. Molecular basis for the preferential cleft recognition by dromedary heavy-chain antibodies. Proc Natl Acad Sci USA 103: 4586–4591.

Decock J, Thirkettle S, Wagstaff L, Edwards DR. 2011. Matrix metalloproteinases: Protective roles in cancer. J Cell Mol Med 15:1254–1260.

Deryugina EI, Ratnikov B, Monosov E, Postnova TI, DiScipio R, Smith JW, Strongin AY. 2001. MT1-MMP initiates activation of pro-MMP-2 and integrin αvβ3 promotes maturation of MMP-2 in Breast carcinoma cells. Exp Cell Res 263:209–223.

Desmyter A, Transue TR, Ghahroudi MA, Thi MH, Poortmans F, Hamers R, Muyldermans S, Wyns L. 1996. Crystal structure of a camel single-domain VH antibody fragment in complex with lysozyme. Nat Struct Biol 3:803–811.

Devy L, Huang L, Naa L, Yanamandra N, Pieters H, Frans N, Chang E, Tao Q, Vanhove M, Lejeune A, van Gool R, Sexton DJ, Kuang G, Rank D, Hogan S, Pazmany C, Ma YL, Schoonbroodt S, Nixon AE, Ladner RC, Hoet R, Henderikx P, Tenhoor C, Rabbani SA, Valentino ML, Wood CR, Dransfield DT. 2009. Selective inhibition of matrix metalloproteinase-14 blocks tumor growth, invasion, and angiogenesis. Cancer Res 69:1517–1526.

Egeblad M, Werb Z. 2002. New functions for the matrix metalloproteinases in cancer progression. Nat Rev Cancer 2:161–174.

Farady CJ, Sun J, Darragh MR, Miller SM, Craik CS. 2007. The mechanism of inhibition of antibody-based inhibitors of membrane-type serine protease 1 (MT-SP1). J Mol Biol 369(4):1041–1051.

Fernandez-Catalan C, Bode W, Huber R, Turk D, Calvete JJ, Lichte A, Tschesche H, Maskos K. 1998. Crystal structure of the complex formed by the membrane type 1-matrix metalloproteinase with the tissue inhibitor of metalloproteinases-2, the soluble progelatinase A receptor. EMBO J 17(17):5238–5248.

Forsman A, Beirnaert E, Aasa-Chapman M, Hoorelbeke B, Hijazi K, Koh W, Tack V, Szynol A, Kelly C, McKnight A, Verrips T, Haard H, Weiss R. 2008. Llama antibody fragments with cross-subtype human immunodeficiency virus type 1 (HIV-1)-neutralizing properties and high affinity for HIV-1 gp120. J Virol 82 (24):12069–12081.

Georgiou G, Ippolito GC, Beausang J, Busse CE, Wardemann H, Quake SR. 2014. The promise and challenge of high-throughput sequencing of the antibody repertoire. Nat Biotechnol 32:158–168.

Gingras D, Bousquet-Gagnon N, Langlois S, Lachambre M, Annabi B, Beliveau R. 2001. Activation of the extracellular signal-regulated protein kinase (ERK) cascade by membrane-type-1 matrix metalloproteinase (MT1-MMP). FEBS 507:231–236.

Golubkov VS, Chekanov AV, Doxsey SJ, Strongin AY. 2005. Centrosomal pericentrin is a direct cleavage target of membrane type-1 matrix metalloproteinase in humans but not in mice. J Biol Chem 280:42237–42241.

Kajita M, Itoh Y, Chiba T, Mori H, Kinoh AO, Seiki M. 2001. Membrane-type 1 matrix metalloproteinase cleaves CD44 and promotes cell migration. J Cell Biol 153:893–904.

Kessenbrock K, Plaks V, Werb Z. 2010. Matrix metalloproteinases: Regulators of the tumor microenvironment. Cell 141(1):52–67.

Kridel SJ, Sawai H, Ratnikov BI, Chen EI, Li W, Godzik A, Strongin AY, Smith JW. 2002. A unique substrate binding mode discriminates membrane type-1 matrix metalloproteinase from other matrix metalloproteinases. J Biol Chem 26: 23788–23793.

Lauwereys M, Ghahroudi MA, Desmyter A, Kinne J, Hölzer W, De Genst E, Wyns L, Muyldermans S. 1998. Potent enzyme inhibitors derived from dromedary heavy-chain antibodies. EMBO J 17(13):3512–3520.

Lawrence MS, Phillips KJ, Liu DR. 2007. Supercharging proteins can impart unusual resilience. J Am Chem Soc 129:10110–10112.

Margulies M, Egholm M, Altman WE, Attiya S, Bader JS, Bemben LA, Berka J, Braverman MS, Chen YJ, Chen Z, Dewell SB, Du L, Fierro JM, Gomes XV, Godwin BC, He W, Helgesen S, Ho CH, Irzyk GP, Jando SC, Alenquer ML, Jarvie TP, Jirage KB, Kim JB, Knight JR, Lanza JR, Leamon JH, Lefkowitz SM, Lei M, Li J, Lohman KL, Lu H, Makhijani VB, McDade KE, McKenna MP, Myers EW, Nickerson E, Nobile JR, Plant R, Puc BP, Ronan MT, Roth GT, Sarkis GJ, Simons JF, Simpson JW, Srinivasan M, Tartaro KR, Tomasz A, Vogt KA, Volkmer GA, Wang SH, Wang Y, Weiner MP, Yu P, Begley RF, Rothberg JM. 2005. Genome sequencing in microfabricated high-density picolitre reactors. Nature 437:376–380.

Metzker ML. 2010. Applications of next-generation sequencing technologies—The next generation. Nat Rev Genetics 11:31–46.

Nagase H. 2001. Matrix metalloproteinase inhibitors in cancer therapy. In: Clendeninn NJ, Appelt K, editors. Substrate specificity of MMPs. Cancer drug discovery and development. PL: Springer. p 39–66.

Nam D, Ge X. 2015. Direct production of functional matrix metalloproteinase-14 without refolding or activation and its application for in vitro inhibition assays. Biotechnol Bioeng 113(4):717–723.

Nam DH, Rodriguez C, Remacle AG, Strongin AY, Ge X. 2016. Active-site MMP-selective antibody inhibitors discovered from convex paratope synthetic libraries. Proc Natl Acad Sci USA 113(52):14970–14975.

Naqid IA, Owen JP, Maddison BC, Spiliotopoulos A, Emes RD, Warry A, Tchórzewska MA, Martelli F, Gosling RJ, Davies RH, Ragione RM, Gough KC. 2016. Mapping polyclonal antibody responses to bacterial infection using next generation phage display. Sci Rep 6:24232.

Nieba L, Honegger A, Krebber C, Plückthun A. 1997. Disrupting the hydrophobic patches at the antibody variable/constant domain interface: Improved in vivo folding and physical characterization of an engineered scFv fragment. Protein Eng 10(4):435–444.

Overall CM, Kleifeld O. 2006. Validating matrix metalloproteinases as drug targets and anti-targets for cancer therapy. Nat Rev Cancer 6:227–239.

Pushkarev D, Neff NF, Quake SR. 2009. Single-molecule sequencing of an individual human genome. Nat Biotechnol 27:847–850.

Ravn U, Didelot G, Venet S, Ng KT, Gueneau F, Rousseau F, Calloud S, Kosco-Vilbois M, Fischer N. 2013. Deep sequencing of phage display libraries to support antibody discovery. Methods 60(1):99–110.

Ravn U, Gueneau F, Baerlocher L, Osteras M, Desmurs M, Malinge P, Magistrelli G, Farinelli L, Kosco-Vilbois MH, Fischer N. 2010. By-passing in vitro screening-next generation sequencing technologies applied to antibody display and in silico candidate selection. Nucleic Acids Res 38:e193.

Reddy ST, Ge X, Boutz D, Ellington AD, Marcotte EM, Georgiou G. 2011. Rapid isolation of monoclonal antibodies from animals. U.S. Pat. No. 9,090,674.

Reddy ST, Ge X, Miklos AE, Hughes RA, Kang SH, Hoi KH, Chrysostomou C, Hunicke-Smith SP, Iverson BL, Tucker PW, Ellington AD, Georgiou G. 2010. Monoclonal antibodies isolated without screening by analyzing the variable-gene repertoire of plasma cells. Nat Biotechnol 28(9):965–969.

Schneider EL, Lee MS, Baharuddin A, Goetz DH, Farady CJ, Ward M, Wang CI, Craik CS. 2012. A reverse binding motif that contributes to specific protease inhibition by antibodies. J Mol Biol 415:699–715.

Sela-Passwell N, Kikkeri R, Dym O, Rozenberg H, Margalit R, Arad-Yellin R, Eisenstein M, Brenner O, Shoham T, Danon T, Shanzer A, Sagi I, . 2011. Antibodies targeting the catalytic zinc complex of activated matrix metalloproteinases show therapeutic potential. Nat Med 18:143–147.

Smith AJ. 2015. New horizons in therapeutic antibody discovery: Opportunities and challenges versus small-molecule therapeutics. J Biomol Screen 20(4):437–453.

Spinelli S, Frenken L, Bourgeois D, Ron L, Bos W, Verrips T, Anguille C, Cambillau C, Tegoni M. 1996. The crystal structure of a llama heavy chain variable domain. Nat Struct Biol 3:752–757.

Turk B. 2006. Targeting proteases: Successes, failures and future prospects. Nat Rev Drug Discov 5:785–799.

Turner KB, Naciri J, Liu JL, Anderson GP, Goldman ER, Zabetakis D. 2016. Next-generation sequencing of a single domain antibody repertoire reveals quality of phage display selected candidates. PLoS ONE 11(2):e1149393.

Udi Y, Grossman M, Solomonov I, Dym O, Rozenberg H, Moreno V, Cuniasse P, Dive V, Arroyo A, Sagi I,. 2015. Inhibition mechanism of membrane metalloprotease by an exosite-swiveling conformational antibody. Structure 23:104–115.

Zarrabi K, Dufour A, Li J, Kuscu C, Pulkoski-Gross A, Zhi J, Hu Y, Sampson N, Zucker S, Cao J. 2011. Inhibition of matrix metalloproteinase 14 (MMP-14)-mediated cancer cell migration. J Biol Chem 286:33167–33177.

Zhu J, Ofek G, Yang Y, Zhang B, Louder MK, Lu G, McKee K, Pancera M, Skinner J, Zhang Z, Parks R, Eudailey J, Lloyd KE, Blinn J, Alam SM, Haynes BF, Simek M, Burton DR, Koff WC, Comparative Sequencing Program NISC, Mullikin JC, Mascola JR, Shapiro L, Kwong PD. 2013. Mining the antibodyome for HIV-1-neutralizing antibodies with next-generation sequencing and phylogenetic pairing of heavy/light chains. Proc Natl Acad Sci USA 110 (16):6470–6475.

Zucker S, Cao J. 2009. Selective matrix metalloproteinase (MMP) inhibitors in cancer therapy: Ready for prime time? Cancer Biol Ther 8:2371–2373.

Supporting Information

Additional supporting information may be found in the online version of this article at the publisher's web-site.

Supporting Information

Identification of Highly Selective MMP-14 Inhibitory Fabs by Deep Sequencing

Tyler Lopez, Dong Hyun Nam, Evan Kaihara, Zahid Mustafa, Xin Ge*

Department of Chemical and Environmental Engineering, University of California, Riverside, 900 University Ave, Riverside, CA 92521; * Correspondence to: xge@engr.ucr.edu

MATERIALS AND METHODS:

Long CDR-H3 library generation. Six degenerate polynucleotides were synthesized (IDT) to encode randomized CDR-H3s having 23, 25, or 27 aa and partial framework region 3 (FR3) and FR4. For CDR-H3 with 23 aa, XYZ codons were used, which contained unequal nucleotide ratios at each position of the codon triplet (X = 38% G, 19% A, 26% T and 17% C; Y = 31% G, 34% A, 17% T and 18% C; and Z = 24% G and 76% C). For CDR-H3 with 25 or 27 aa, NNS codons were used. After assembly CDR-H3 genes were gel purified using DNA recovery kit (Zymo Research), digested with AflII/HindIII and inserted into a β-lactamase fusion vector pVH-bla to remove stop codons and reading-frame shifted CDR-H3 fragments as previously described (Seehaus *et al.*, 1992; Lutz *et al.*, 2002). To construct Fab phagemid libraries, the cells containing CDR-H3-23, -25 and -27 libraries were grown overnight at 30 ^{o}C followed by plasmid DNA extraction and digestion with AflII/BsmBI. The phagemids of a synthetic Fab antibody library with >10^{10} variants (Persson *et al.*, 2013) were amplified and digested using the same REs. The fragments of Fab phagemids and CDR-H3 were ligated and transformed into E. coli XL1-Blue by electroporation (Nam *et al.*, 2016).

Phage panning of the long-CDR-H3 library against cdMMP-14. Synthetic antibody Fab phage libraries (1.25×10^{9} variants in the original un-panned library) carrying extended CDR-H3 (23-27 amino acids) were subjected to three rounds of panning against the catalytic domain of MMP-14 (cdMMP-14), which was recombinantly expressed (Nam and Ge, 2015), purified, biotinylated, and immobilized on ELISA plates via biotin-BSA and streptavidin. To ensure full coverage of the library diversity, Fab phagemid transformed cells equivalent to over 10 folds of the library size (>1.2×10^{10} cells) were inoculated for phage propagation before the initial round of panning. The bound phages were washed with increasing stringency (5-20 washing times) over the course of the three rounds of panning. Bound phages were eluted using purified n-TIMP-2, a native inhibitor of MMP-14. And eluted phages were introduced to freshly prepared XL1-Blue cells for propagation.

RESULTS:

Monoclonal phage ELISA yielded a panel of binding and inhibitory antibodies. 288 phage-Fab clones from the second and the third rounds were screened by monoclonal phage ELISA. 126 clones (44% hit rate) showed high ELISA signals (ratio of cdMMP-14

to streptavidin > 5) 77 high signal clones were subjected to Sanger DNA sequencing and 20 unique clones carrying long CDR-H3 were found. The inhibitory potency against MMP-14 was tested using FRET peptide substrate. 13 Fabs showed an inhibition with potencies between 10 nM and 5 μM (Nam *et al.*, 2016).

REFERENCES:

Lutz S, Fast W, Benkovic SJ. 2002. A universal, vector-based system for nucleic acid reading-frame selection. Protein Eng. 15:1025-1030.

Persson H, Ye W, Wernimont A, Adams JJ, Koide A, Koide S, Lam R, Sidhu SS. 2013. CDR-H3 diversity is not required for antigen recognition by synthetic antibodies. J. Mol. Biol. 425:803-811.

Seehaus T, Breitling F, Dubel S, Klewinghaus I, Little M. 1992. A vector for the removal of deletion mutants from antibody libraries. Gene. 114:235-237.

Nam D, Ge X. 2015. Direct production of functional matrix metalloproteinase -14 without refolding or activation and its application for in vitro inhibition assays. Biotechnol. Bioeng. 113(4):717-723.

Nam DH, Rodriguez C, Remacle AG, Strongin AY, Ge X. 2016. Active-site MMP-selective antibody inhibitors discovered from convex paratope synthetic libraries. Proc Natl Acad Sci USA. 113 (52):14970-14975.

SI TABLES:

Table S1. Frequency analysis of the 20 MMP-14 binding clones identified by ELISA in previous study (Nam et al., 2016).

ID by ELISA	ID by NGS	CDR-H3 Sequence (Length)	Og (%)	R1 (%)	R2 (%)	R3 (%)	Binding Affinity	Inhibition Potency
3A2	R3C9	VKLQKDKSHQWIRNLVATPYGRYVMDY(27)	0	0	0.01	**0.29**	3.8 nM	9.7 nM
3E2	-	GIKGLVFTGSQMKMLRRGNYNWYVMDY(27)	0	0	0	0.03	47 nM	42 nM
3D9	-	RLMAYHGSCSSRLCQTAISPQRYAMDY(27)	0	0	0.01	0.04	6.4 nM	61 nM
2B5	-	IGVNAWAVKMSQRMLATRGSGWYVMDY(27)	0	0	0	0.03	24 nM	240 nM
3G9	-	ATNEKFRRKSLQVRLLMRSWLAYAMDY(27)	0	0	0.01	0.04	160 nM	390 nM
33D2	-	SKYGPASRQLASRTSWSGPRGKYGMDY(27)	0	0	0	0	120 nM	420 nM
3F3	R2C13	LYNGWLMVEGIGSAREGPTWYAMDY(25)	0	0	**0.03**	0.09	34 nM	970 nM
33F3	R2C2	GVRGNKLRLLSSRSGLMESHYVMDY(25)	0	0	**0.12**	1.66	1.0 μM	2.3 μM
33D4	R2C15	SVHMKLSNKILSGWSWNNSFYAMDY(25)	0	0	**0.03**	0.07	460 nM	3.9 μM
32D1	-	MSLHRNFNQQGRSRLLGRMPRTYGMDY(27)	0	0	0	0.04	350 nM	4.2 μM
3A6	-	RPCKACRTRLELVRRGMDSGLRYGMDY(27)	0	0	0	0.05	980 nM	4.2 μM
33C4	R2C3	PTTSRVNKKLFRVSVLHPGSYGMDY(25)	0	7.99E-03	**0.11**	0.61	220 nM	4.6 μM
3E9	-	NGRYPGFLKRAHKRLLNFKAYVMDY(25)	0	0	0.01	0.01	51 nM	6.0 μM
32C2	-	SQHAKKSTIIRMLEHQSRSGMQYVMDY(27)	0	0	0	0.01	150 nM	8.0 μM
32E10	R2C19	LDRDRYIHVGRAGNTYSNYYYVMDY(25)	0	7.99E-03	**0.03**	0.17	9.7 nM	-
32C11	R3C7	EIHMLSRQARYLRDGRRPRGSMYVMDY(27)	0	0	0.01	**0.33**	29 nM	-
2H9	-	GTSFQVRCVLYRLLSPGRYVMDY(23)	0	0	0	0.02	120 nM	-
3B2	R2C1	STAATTLSRMSRSYWTIQLPYGMDY(25)	0	0	**0.13**	1.89	590 nM	-
2E4		SARLRLRGNHDRRRSKSVYYRPYVMDY(27)	0	0	0	0	840 nM	-
33F5	R2C20	NFRVESAGRPGKTVLRKDGKYAMDY(25)	0	0	**0.03**	0.47	1.6 μM	-

Notes:

1. Binding affinity and inhibition IC_{50} data were from previous study [Nam et al., 2016]. Clones are ranked by their inhibition potencies or binding affinities for non-inhibitory clones.
2. All these clones have zero copies in Og. In R1, except R2C3 and R2C19 have one copy, all other clones have zero copies.

SI FIGURES:

Figure S1:

A

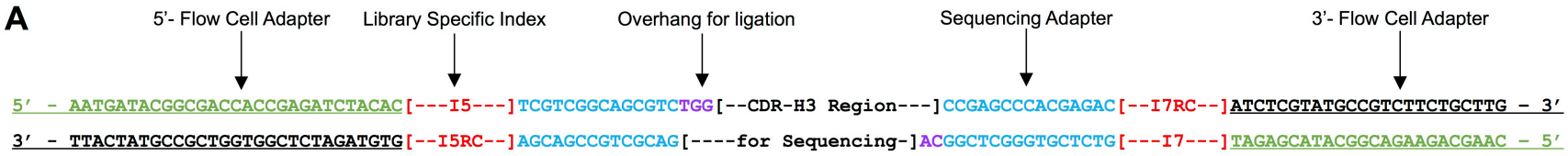

B

	I5 Index		I7 Index	
Library	Name	Sequence	Name	Sequence
Og	[N/S/E]501	TAGATCGC	N703	AGGCAGAA
R1	[N/S/E]502	CTCTCTAT	N704	TCCTGAGC
R2	[N/S/E]503	TATCCTCT	N709	GCTACGCT
R3	[N/S/E]504	AGAGTAGA	N710	CGAGGCTG

Figure S1. Custom-designed primers for Illumina sequencing. **(A)** Diagram of the full-length sequencing samples with four primers showing functions of each segment. Double-stranded upstream and downstream adapters were assembled by annealing primers via gradient cooling. The flow cell adapter is for binding to the surface of sequencing channels in flow cells. The index allows de-multiplexing of the libraries for accurate analysis and reduction of batch-to-batch variations. I5RC and I7RC represent the reverse compliments of the I5 and I7 index respectively. The sequencing adapters correspond to the sequencing primer used in MiSeq analysis. A high melting temperature is chosen to avoid de-associating the primers during the sequencing runs. The 3'-overhangs allow direct ligation of the digested double-stranded CDR-H3 DNA with adapters for sample preparation without PCR amplification. **(B)** Indexes used for each library. The I5 and I7 indexes are for the upstream and downstream adapters respectively, and chosen to maintain a 1:1 ratio of (A+C) : (G+T).

Figure S2:

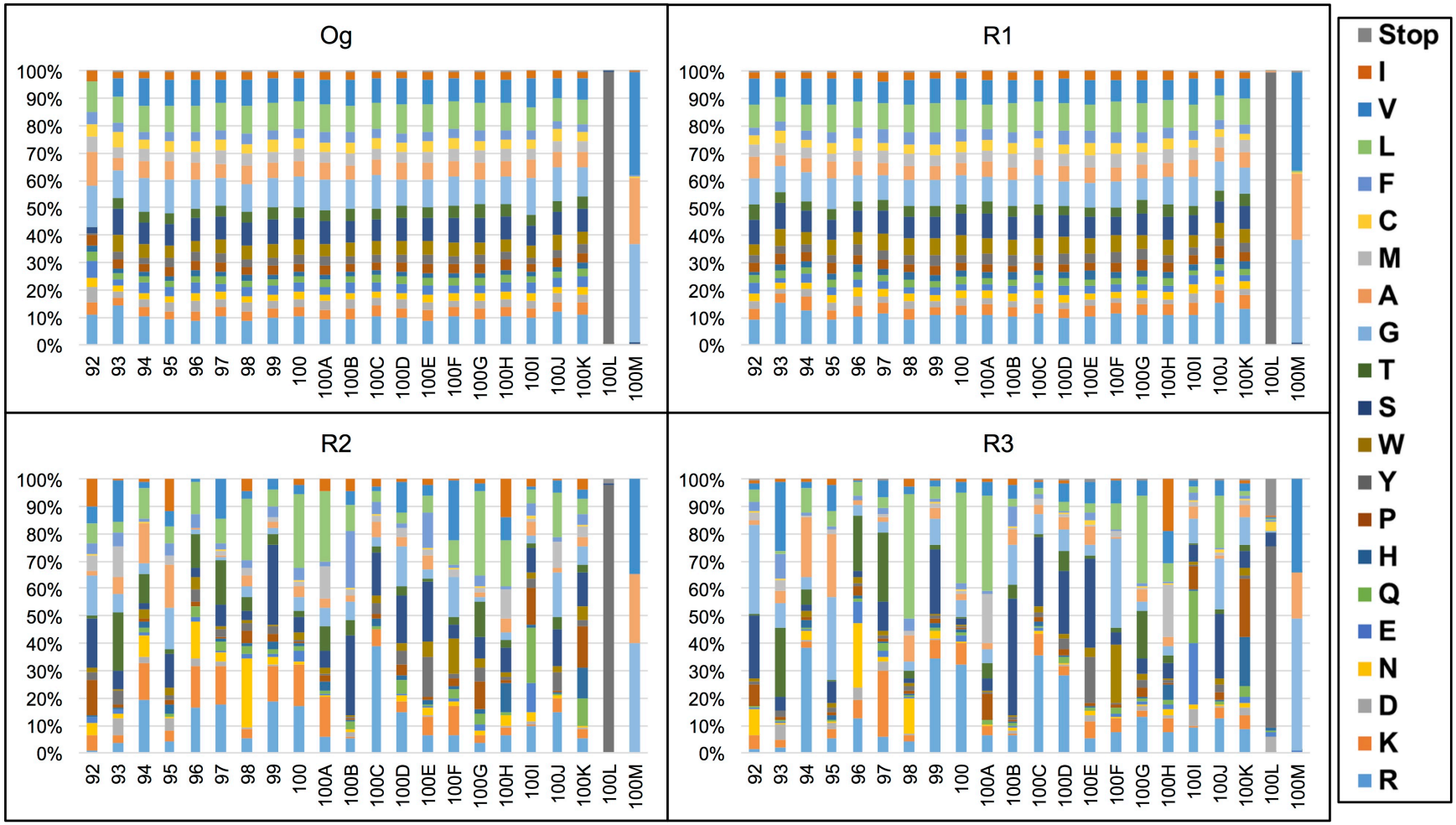

Figure S2. Analysis of amino acid usage at each position of CDR-H3s. The even distribution in the original library is indicative of high quality of the constructed library as designed. The usage distribution dramatically altered over the course of phage panning. CDR-H3s with 25 aa in length were used as an example for analysis.

Figure S3:

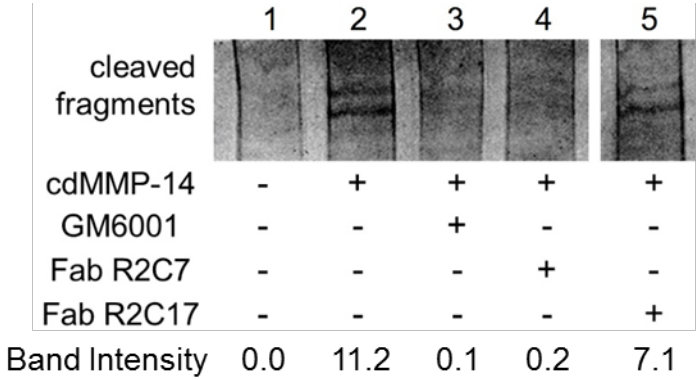

Figure S3. Zymography studies showing Fab R2C7 inhibits cdMMP-14 from degrading gelatin. 10 nM cdMMP-14 with 1 mg/mL gelatin was incubated in the presence or absence of the inhibitor of interest, and processed by 12% SDS-PAGE gel. Lane 1, no cleaved fragments without cdMMP-14; Lane 2, cleavage of gelatin by cdMMP-14; Lane 3, GM6001 inhibited cdMMP-14 from cleaving gelatin; Lane 4, Fab R2C7 inhibited cdMMP-14 from cleaving gelatin; Lane 5, non-inhibitory Fab R2C17 lacked function to block cdMMP-14. Relative intensities of the bands associated with cleaved fragments were shown in the last row (background intensity in Lane 1 was set as zero).

Figure S4:

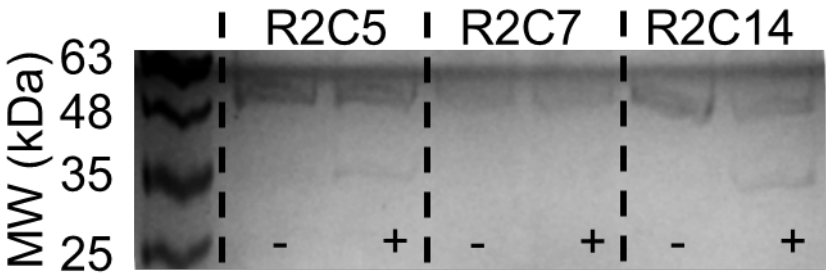

Figure S4. Identification of suicide inhibitors. 1 μM Fabs R2C5, R2C7 and R2C14 were incubated in the presence (+) or absence (-) of 200 nM cdMMP-14 for 2 hours at room temperature then analyzed by 12% SDS-PAGE. Truncated R2C5 and R2C14 fragments were observed while R2C7 was resistant to be cleaved by cdMMP-14.

Figure S5:

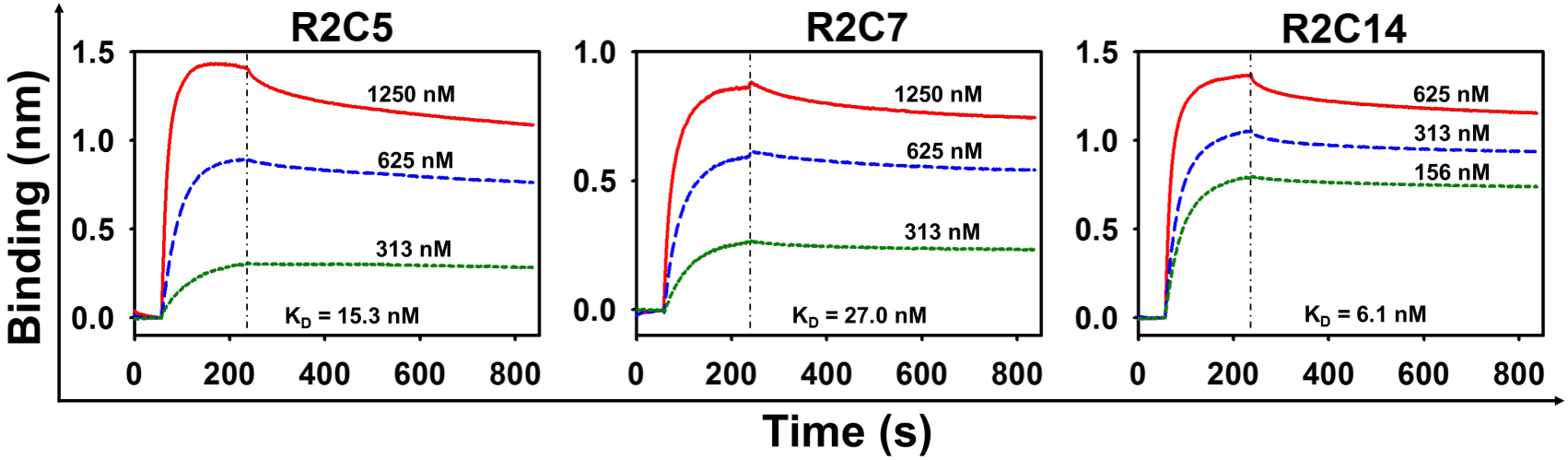

Figure S5. Binding kinetics measurements of Fabs R2C5, R2C7, and R2C14 by bio-layer interferometry. Using ForteBio BLItz system, biotinylated cdMMP-14 was loaded onto a streptavidin biosensor for 60 sec to establish baselines. Fabs were introduced at a variety of concentrations and their association to immobilized cdMMP-14 was monitored for 3 min then allowed to dissociate into 50 mM HEPES (pH 6.8) for 10 min (change to dissociation is indicated by the vertical black dashed line). Determined k_{on} and k_{off} parameters were used to calculate K_D values.